Numerical Investigation of Supersonic Annular Flow About Struts of Various Thicknesses

G. J. Harloff*
Sverdrup Technology, Inc., Brook Park, Ohio 44142
and
K. E. Williams† and F. B. Gessner‡
University of Washington, Seattle, Washington 98195

Introduction

THE objective of this numerical study is to investigate flow development in the vicinity of a strut (finite-length fin) of various thicknesses that intersects curved endwalls with well-developed turbulent boundary layers for weak-to-strong interaction strengths. To accomplish this, four diamond-shaped, symmetric struts were placed circumferentially equidistant in an annular flow passage with a steady supersonic core flow. This type of application may exist, for example, in dual combustion ramjets with supersonic annular flow[1] or other configurations where struts are needed between the cowl and centerbody. The current investigation extends previous studies by Williams et al.[2,3] by examining the influence of strut thickness on interaction phenomena induced by each strut configuration. The interactions occur in an annular flow passage with convex and concave curved endwalls for the inner and outer walls, respectively, and include the effect of crossing shocks between struts. The inner-to-outer wall radius ratio is 0.7, the annular gap-to-strut chord ratio is 0.7, and the strut chord is 2.54 cm long. The maximum thickness of the struts examined includes 0.125, 0.188, 0.25, and 0.5 chord lengths, which corresponds to strut half-angles of 7, 11, 14, and 26.5 deg, respectively. The contraction ratios for the four 14- and 26.5-deg struts, 1.09 and 1.19, respectively, are less than the maximum permissible value for Mach 3 of 1.39, so that these supersonic flows can be established experimentally. The turbulent boundary layers on the walls of the annular duct are roughly 0.15 strut chords thick at a location 0.5 chords upstream of the strut and the "inviscid" core has a nominal Mach number of 3.0. The calculations were made at a Reynolds number based on the strut chord of 3×10^5.

Numerical Approach

The PARC3D[4] flow solver was used for the computations. It solves the full Reynolds-averaged Navier–Stokes equations in strong conservation form. Closure was obtained by applying the Baldwin–Lomax[5] turbulence model near walls and the Thomas[6] turbulence model in the wake region. The grids were created using GRIDGEN[7] with the first grid point away from the strut and the inner and outer walls at or below $y^+ = 1.0$ based on the undisturbed boundary-layer profiles. The computational control volume extends circumferentially from 0 deg at the strut centerline to a plane of symmetry at 45 deg and from 0.5 chords upstream of the strut to 5 chords downstream of the strut trailing edge. Boundary conditions include adiabatic no slip on the duct walls and on the strut, symmetry conditions on the 0- and 45-deg planes, and extrapolated properties at the exit plane. The inlet conditions were obtained from axisymmetric calculations and were fixed; see Ref. 2. Coarse grids of $73 \times 35 \times 35$ were used for all of the strut angles, and fine grids of $147 \times 75 \times 75$ were used for the 7- and 14-deg struts to study grid resolution effects on the solution. The fine grid flowfields only are presented for the 7- and 14-deg struts. These grids were further adapted to pressure gradients for the particular solutions using MAG3D[8] because of the complex flow phenomena considered here. The rectangular reference lines on the surfaces of most of the figures in this paper are located at axial locations (relative to the leading edge of the strut in chord lengths) of −0.5, 0.0 (strut leading edge), 0.5, 1.0 (strut trailing edge), 2.0, 3.0, 4.0, 5.0, and 6.0 and at circumferential locations of 0, 15, 30, and 45 deg from the strut centerline.

Results

Flow Structure

Particle trajectory paths, for particles injected in the strut centerline inflow boundary layer, generally follow limiting wall streamline paths beneath the horseshoe vortex that is generated at the strut leading edge. These particle path lines are indicated in Figs. 1a–1d for the 7-, 11-, 14-, and 26.5-deg struts, respectively. As the strut half-angle increases, the leading- and trailing-edge shocks strengthen, and the leading-edge horseshoe vortex migrates more rapidly toward the 45-deg symmetry plane. Figures 1a–1d also show that there is an upward sweep of particle pathlines away from the centerbody along the expansion face of the strut. Some of these particles originate in the corner vortex formed along the intersection of the strut compression face with the centerbody. Their paths are indicative of the path taken by the compression face corner vortex before it is convected into the wake. Similar behavior is observed for particles originating in the compression face corner vortex formed at the strut/cowl intersection, noting that these particles are deflected downward away from the cowl along the expansion face of the strut. The net result is a pair of counter-rotating vortices in the wake on each side of the strut plane of symmetry that are roughly centered about the curved midplane between the cowl and centerbody. Although it is not clearly evident in Fig. 1, additional corner vortices are formed along the intersection of the strut expansion face with the cowl and centerbody surfaces. These vortices merge with horseshoe vortices formed at the strut trailing edge as a result of the recompression process. The origin and evolution of these vortices is described in more detail by Williams et al.[3]

Total pressure contours on the strut symmetry plane and on the exit plane of the computational domain are also shown in Fig. 1 for the four struts examined. In this figure the numerical values correspond to P_t/P_{t0}, where P_t is total pressure and P_{t0} is the inlet total pressure. The total pressure field at the domain exit has an obvious deficit behind the strut, and this deficit increases as the strut half-angle increases. The low total pressures in the strut plane of symmetry are due to both viscous wake losses and the entrainment of low-energy boundary-layer fluid near the strut expansion face. The growth of the viscous wake is underpredicted,[3] compared with experiment, for the 7-deg strut and presumably for the other struts as well. This deficiency is probably due to weaknesses of the wake turbulence model employed. For the 26.5-deg strut, a large region of low-energy flow is predicted behind the strut at the domain exit; see Fig. 1d. This is partly due to boundary-layer flow separation on the expansion face of the strut. For this strut, the endwall boundary layers also separate upstream of the leading-edge horseshoe vortex. Boundary-layer flow separation details may not be accurate due to limitations of the turbulence models employed.

Static pressure distributions on the curved duct midplane are illustrative of inviscid flowfield behavior in the core flow before viscous effects are felt at this location. Shock wave locations can be discerned by observing the static pressure contours, P/P_0, as shown in Fig. 2, where P is static pressure and P_0 is the inlet static pressure. For the 7-deg strut, the leading- and trailing-edge shocks are readily observed in Fig. 2a (flow is left to right), and the leading-edge shock wave from the neighboring strut is observed to cross the trailing-edge shock wave about 3 chords downstream from the strut trailing edge. The expansion fan, which originates at the strut midpoint, is also evident in Fig. 2a, and it begins to overtake the leading-

Presented as Paper 93-2927 at the AIAA 24th Fluid Dynamics Conference, Orlando, FL, July 6–9, 1993; received May 26, 1994; revision received Dec. 1, 1994; accepted for publication Dec. 1, 1994.

*Senior Staff Scientist, NASA LeRC Group; currently Senior Engineer, NYMA, Inc., Brook Park, OH 44142. Associate Fellow AIAA.

†Graduate Research Associate, Department of Mechanical Engineering. Student Member AIAA.

‡Professor, Department of Mechanical Engineering. Member AIAA.

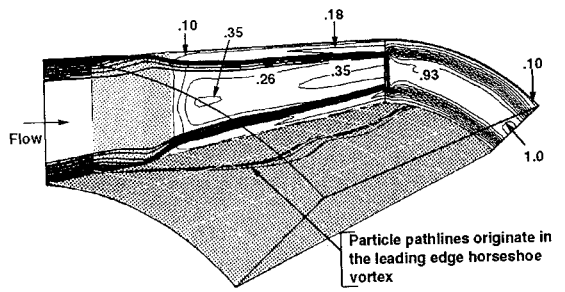

a) 7-deg strut

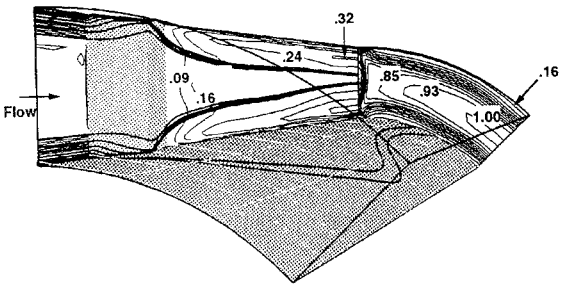

b) 11-deg strut

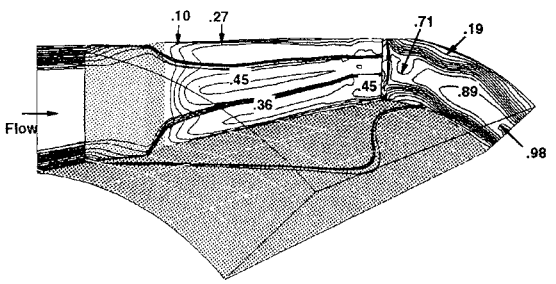

c) 14-deg strut

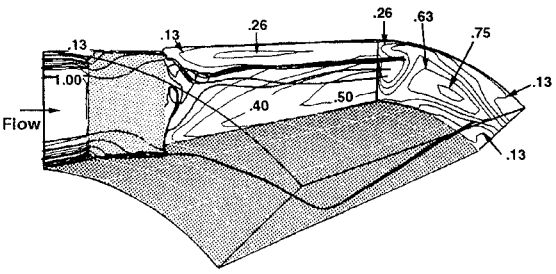

d) 26.5-deg strut

Fig. 1 Particle trajectories and total pressure contours.

edge shock 0.5 chords from the trailing edge at about 23 deg from the strut centerline. The maximum pressure rise on the 45-deg plane of symmetry (domain boundary) is of interest, because streamwise boundary-layer separation may occur due to the added pressure rise associated with crossing shocks. For the 7-deg strut the maximum static pressure ratio at the intersection of the leading-edge shocks on the 45-deg symmetry plane is 2.44 (the highest value of pressure does not necessarily correspond to the peak contour plotted in Fig. 2a because the extreme value is determined for a volume and the contours are plotted in planes). The midplane static pressure distributions for the 11-, 14-, and 26.5-deg struts are presented in Figs. 2b–2d, respectively. Similar shock and expansion fan flow features are observed for the 11- and 14-deg struts. The resolution for the 11- and 26.5-deg struts is lower since the solutions were computed using fewer grid points (89,425 for the 11- and 26.5-deg struts vs 826,875 for the 7- and 14-deg struts). The 26.5-deg strut pressure field is very different, and as discussed later, large-scale boundary-layer separation is evident.

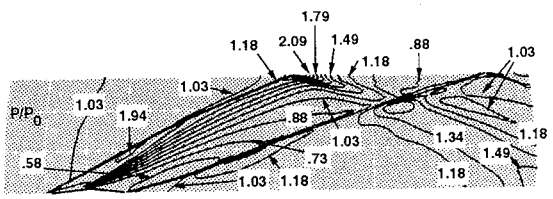

a) 7-deg strut

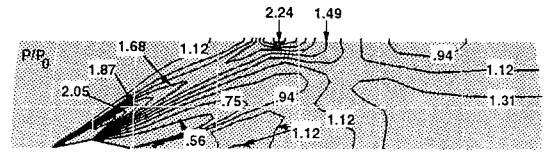

b) 11-deg strut

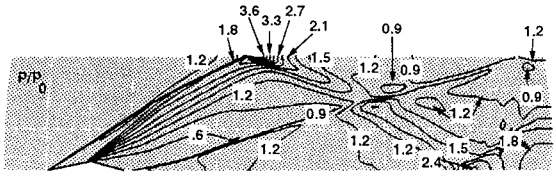

c) 14-deg strut

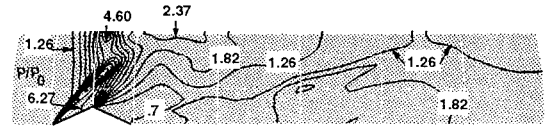

d) 26.5-deg strut

Fig. 2 Midplane static pressure distributions.

Wall static pressures and limiting streamline distributions on the centerbody for the four strut configurations are shown in Figs. 3a–3d. The cowl pressure fields and streamlines are similar except near the crossing shock location where local flow separation occurs (on the cowl) for the 14-deg strut. These distributions are not shown due to space limitations. Near the leading-edge shock the centerbody pressure gradients are weaker than midplane pressure gradients due to viscous dissipation effects in the boundary layer that diffuse the pressure jump. The extent of the upstream influence (initial streamline deflection from the freestream direction) within the boundary layer in front of the strut, compared with the inviscid midplane shock front, is about one-half chord length at 15 deg from the strut centerline. As observed, the limiting streamlines follow the pressure rise contours very closely and turn downstream with it (see Figs. 3a–3d). The limiting streamlines indicate that the particle pathlines turn toward the strut centerline as a result of the expansion fan turning the flow back toward the strut centerline. For the 7-deg strut, Fig. 3a shows that downstream of the strut (by two chords and about 18 deg from the strut centerline) limiting streamlines turn toward the 45-deg plane of symmetry due to the influence of the trailing-edge shock wave. The streamlines are turned back toward the strut centerline at three chord lengths near 20 deg due to the pressure increase caused by the leading-edge shock reflection at the 45-deg plane of symmetry. As the strut half-angle increases, limiting streamlines initially near the leading edge approach the 45-deg symmetry plane for the 14-deg strut, as shown in Fig. 3c. The reflected shock at 45 deg turns the boundary-layer flow back toward the strut centerline. The pressure variations are higher on the cowl because the concave surface increases the strength of compression and expansion waves due to wave reinforcement, and, similarly, the pressure variations are lower on the centerbody because the convex surface decreases the strength of the waves as a result of wave expansion effects. For the 7-deg strut, the maximum pressures, P/P_0, on the 45-deg symmetry plane are 1.55 and 1.69 for the centerbody and cowl, respectively.

Previous studies have interpreted the convergence of wall streamlines into a coalescence line as an indication of separated flow.

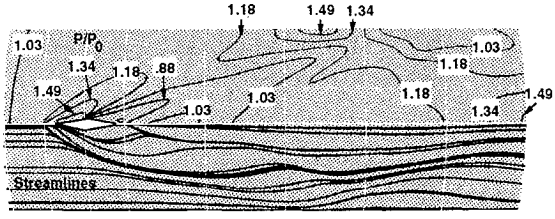

a) 7-deg strut

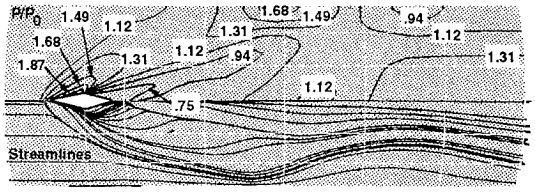

b) 11-deg strut

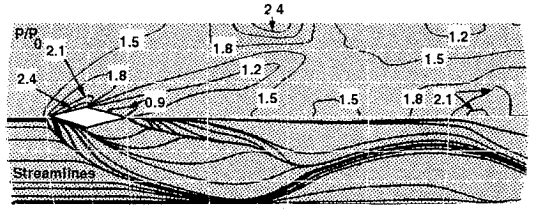

c) 14-deg strut

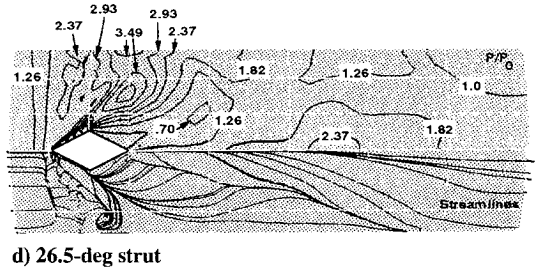

d) 26.5-deg strut

Fig. 3 Centerbody static pressure distributions and limiting streamlines.

Horseshoe vortices formed near the strut leading and trailing edges are each bounded by a coalescense line. The leading-edge vortex entrains boundary-layer fluid; the entrained flow accounts for higher shear stress at the wall under the vortex, as confirmed by oil flow visualization results,[3] and diminishes the flow energy through viscous dissipation. The compression face corner vortex entrains low-energy boundary-layer fluid, which is convected up the strut expansion face toward the duct midplane, and adds low-energy fluid into the strut wake, as illustrated by the total pressure contours in Figs. 1a–1d. In reference to Fig. 1, it can be seen that the leading-edge horseshoe vortex has traveled progressively farther away from the 26.5-deg strut than for the 7- or 14-deg strut cases. For the 26.5-deg strut, this vortex reaches the 45-deg plane of symmetry between struts and lifts off the centerbody surface, as implied by the static pressure distributions and limiting streamline patterns in Fig. 3d. This vortex lift off is associated with a severe separation cell that encompasses the entire width of the flow domain in front of the horseshoe vortex. Large-scale boundary-layer separation is also present on the cowl surface that is not shown here.

Conclusions

A numerical study of supersonic flow about struts of various thicknesses in an annular duct has been conducted. The strut thicknesses evaluated were 0.125, 0.188, 0.25, and 0.5 strut chord lengths that correspond to strut half-angles of 7, 11, 14, and 26.5 deg, respectively. In reference to vortical flow behavior, the compression face corner vortex was observed to migrate up the strut expansion face, away from the centerbody. This behavior is important because this vortex, once downstream of the trailing edge, dominates the viscous wake of the strut. Similar behavior was observed for the corner vortex generated at the cowl–strut intersection. An expansion face vortex has also been identified on the centerbody surface.[3] The formation of a recompression vortex was noted at the trailing edge of the strut. This vortex rotates in the same direction as the leading-edge vortex and is formed by mechanisms similar to those that form the leading-edge vortex.[3] For the strongest interaction studied, the 26.5-deg half-angle strut, these vortices, along with severe boundary-layer separation on the endwalls, dominate the flow. Boundary-layer flow separation with local flow reversal was computed on the cowl surface for the 14-deg strut. These results indicate that, for a core flow Mach number of 3.0, struts of less than 14 deg should be used in flight hardware to ensure unseparated boundary-layer flow.

Acknowledgments

This work was supported by the NASA Lewis Research Center under Contract NAS3-25266 and Grant NAG 3-376. David O. Davis was the project monitor. The computations were performed on the NAS Cray Y-MP at NASA Ames. The authors gratefully acknowledge NASA's support of this research. The assistance of Maryann Johnston is gratefully acknowledged.

References

[1]Stockbridge, R. D., "Experimental Investigation of Shock Wave Boundary-Layer Interactions in an Annular Duct," *Journal of Propulsion and Power*, Vol. 5, No. 3, 1989, pp. 346–352.

[2]Williams, K. E., Gessner, F. B., and Harloff, G. J., "Experimental and Numerical Investigation of Supersonic Turbulent Flow in an Annular Duct," *AIAA Journal*, Vol. 32, No. 7, 1994, pp. 1528–1531; also AIAA Paper 93-3123, July 1993.

[3]Williams, K. E., Harloff, G. J., and Gessner, F. B., "Investigation of Supersonic Flow About Strut/Endwall Intersections in an Annular Duct," *AIAA Journal* (to be published).

[4]Cooper, G. K., and Sirbaugh, J. R., "PARC Code: Theory and Usage," Arnold Engineering Development Center, AEDC-TR-89-15, Arnold AFB, TN, 37389, Dec. 1989.

[5]Baldwin, B. S., and Lomax, H., "Thin Layer Approximation and Algebraic Model for Separated Turbulent Flows," AIAA Paper 78-257, Jan. 1978.

[6]Thomas, P. D., "Numerical Method for Predicting Flow Characteristics and Performance of Nonaxisymmetric Nozzles—Theory," NASA CR 3147, Sept. 1979.

[7]Steinbrenner, J. P., Chawner, J. R., and Fouts, C. L., "The Gridgen 3D Multiple Block Grid Generation System," Wright Patterson Development Center, WRDC-TR-90-3022, Wright Patterson AFB, OH, Vols. 1 and 2, July 1990.

[8]Henderson, T., Huang, W., Lee, K., and Choo, Y., "Three-Dimensional Navier–Stokes Calculation Using Solution Adaptive Grids," AIAA Paper 93-0431, Jan. 1993.

Alleviation of Chattering in Flexible Beam Control via Piezofilm Actuator and Sensor

Seung-Bok Choi*
Inha University, Incheon 402-751, Republic of Korea

Introduction

CONSIDERABLE attention has been focused on the development of smart structures with integrated distributed control

Received Jan. 12, 1994; revision received Nov. 9, 1994; accepted for publication Nov. 9, 1994.

*Assistant Professor, Department of Mechanical Engineering, Smart Structures and Systems Laboratory.